Hindawi Publishing Corporation
Journal of Materials
Volume 2016, Article ID 4597271, 15 pages
http://dx.doi.org/10.1155/2016/4597271

Research Article

Influence of Grain Boundary Character and Annealing Time on Segregation in Commercially Pure Nickel

Shery L. Welsh,[1] Monica Kapoor,[2] Olivia D. Underwood,[3] Richard L. Martens,[4] Gregory B. Thompson,[2] and Jeffrey L. Evans[1,5]

[1]*Materials Science Program, University of Alabama in Huntsville, USA*
[2]*Department of Metallurgical & Materials Engineering, The University of Alabama, Tuscaloosa, AL, USA*
[3]*Mechanics of Materials, Sandia National Laboratories, Albuquerque, NM, USA*
[4]*The Central Analytical Facility, University of Alabama, Tuscaloosa, AL, USA*
[5]*Department of Mechanical and Aerospace Engineering, University of Alabama in Huntsville, USA*

Correspondence should be addressed to Shery L. Welsh; slw0013@uah.edu

Received 18 October 2015; Revised 2 January 2016; Accepted 5 January 2016

Academic Editor: Bengt G. Svensson

Commercially pure nickel (Ni) was thermomechanically processed to promote an increase in Σ3 special grain boundaries. Engineering the character and chemistry of Σ3 grain boundaries in polycrystalline materials can help in improving physical, chemical, and mechanical properties leading to improved performance. Type-specific grain boundaries (special and random) were characterized using electron backscatter diffraction and the segregation behavior of elements such as Si, Al, C, O, P, Cr, Mg, Mn, B, and Fe, at the atomic level, was studied as a function of grain boundary character using atom probe tomography. These results showed that the random grain boundaries were enriched with impurities to include metal oxides, while Σ3 special grain boundaries showed little to no impurities at the grain boundaries. In addition, the influence of annealing time on the concentration of segregants on random grain boundaries was analyzed and showed clear evidence of increased concentration of segregants as annealing time was increased.

1. Introduction

Nickel is the major alloying element in some of the most advanced alloys used today in applications ranging from nuclear power plant components to high temperature aircraft engine components [1, 2]. Therefore, studying the character and chemistry of grain boundaries in commercially pure nickel, known as Nickel 200, could help elucidate various fundamental microstructure-property relationships of these materials. Engineering the character and chemistry of grain boundaries in polycrystalline materials can help in improving physical, chemical, and mechanical properties leading to improved performance [3]. However, most of the work done on grain boundary (GB) segregation has been in the modeling and computational arenas [4]. Limited studies exist, which investigate the GB character's influence on segregation behavior at the atomic level for Ni [4].

Segregation, a local enrichment at the GB, can alter the mechanical and physical properties including tensile strength, ductility, and fracture toughness, electrical properties, and so forth [5]. GB structure, as compared to the bulk structure, is very different and exhibits its own unique environment, structure, composition, and energy levels at the atomic level [6]. This GB structure serves to either attract or repel segregants [7]. The process of segregation leads to a decrease in the energy of the system following the thermodynamic principles of Gibbs free energy as the GB tries to attain the lowest energy possible [6, 8, 9]. In addition, preferential interactions also exist between the segregants themselves which can affect segregation behavior [4].

Grain boundaries can be classified as low angle (angle of misorientation <10–15°), high angle, and coincident site lattice (CSL) [10]. CSL boundaries are characterized by misorientations that allow atoms from neighboring lattices to

Table 1: Specimen parameters.

Specimen	GB type	Strain (cold-rolled)	Annealing temperature (°C)	Annealing time (hours)
1	RGB	3%	1000	30
1	SGB	3%	1000	30
2	RGB	3%	1000	1

coincide notionally [11]. The fraction of atoms that coincide at the boundary is called the density of coincidence sites [11]. The reciprocal of this density of the coinciding sites is used to describe a CSL boundary and is designated as Σ [12, 13]. For example, Σ3 boundary will have one-third of the atoms in each of the 2 grains coinciding notionally. Low Σ CSL boundaries, $3 \leq \Sigma \leq 29$, are called special grain boundaries (SGBs) and high Σ CSL boundaries with $\Sigma > 29$ are called random grain boundaries (RGBs) [13, 14]. Σ3, a special boundary, has the largest number of coinciding lattice points which translates into a more ordered structure and lower free volume [8] and GB energy when compared to a random grain boundary [8, 15]. This results in SGBs being slower diffusion pathways [8, 15].

Altering the GB character distribution in a microstructure is known as "GB Engineering" (GBE) [3, 15]. GBE consists of single or multiple thermomechanical processing cycles that include combinations of straining and annealing to alter the distribution of the different types of grain boundaries [3]. Particular processing combinations have been found to produce higher fractions of SGBs which are key to improving material performance [16–18]. It has been shown in several studies that when the fraction of special grain boundaries (Fsp) increased, the resistance to the following properties increased: creep, cavitation, fracture, corrosion, intergranular corrosion, grain boundary sliding, and cracking [8, 19–21]. Grain boundary character distribution (GBCD) characterizes the grain boundaries by providing the fraction of each type of boundary found in the microstructure [10]. Σ3, or special boundary, is the main contributor to GBCD optimization [10, 14].

The above discussion suggests that it is possible to thermomechanically process Ni-based alloys to increase the SGBs which should result in improved segregation resistance to impurities. Most GB studies have focused on models and simulations because experimental studies on segregation are difficult to conduct due to the difficulties in the randomness of sample preparation and experimental procedures, identifying the type-specific GB in such a small volume of material, isolating it for extraction, preparing the sample, and studying it atomically [22]. In order to understand the controlling mechanisms, it is imperative to study them at the atomic level.

A study was designed by the authors to thermomechanically process Ni to promote the formation of SGBs and then atomically investigate the concentration of segregants in SGBs and RGBs. In addition, the effect of increased annealing time on 2 RGBs and their segregation behavior was studied. We utilized electron backscatter diffraction (EBSD) to characterize the grain boundaries and a focused ion beam (FIB) for site-specific lift-out procedure [23] to isolate SGBs and RGBs followed by atom probe tomography (APT). The goal of this research was to study GB segregation behavior experimentally at the atomic level using local electrode atom probe tomography (LEAP).

2. Experimental Procedures

Commercially pure Ni, 3.12 mm thick sheet, was thermomechanically processed to drive segregation [3]. Ni was strained (cold-rolled) to reduce the thickness by 3% followed by annealing at 1000°C in air for 30 hours and 1 hour and was labeled as specimens 1 and 2, respectively. SGB and RGB were extracted from specimen 1 and RGB was extracted from specimen 2. Several attempts were made to extract SGBs from specimen 2 and prepare them for APT analysis but they were unsuccessful. Table 1 shows the thermomechanical processing parameters for each specimen.

EBSD was conducted on JEOL JSM-7000F Field Emission Scanning Electron Microscope (FESEM). The EBSD GB maps were obtained with a step size of 2 microns at 30 kV followed by analyses using the HKL Channel 5 software program where Brandon criterion was applied [24]. EBSD was used to identify the grain boundaries based on their angles of misorientation and provided a map of SGBs and RGBs as shown on the micrographs of Figures 1(a), 1(e), 2(a), and 2(e). Based on CSL statistics, specimen 1 SGB was Σ3 grain boundary with a misorientation angle of approximately 3.575° as the number fraction of Σ3 grain boundaries was 0.34, Σ9 was 0.022, and Σ27a was 0.0038. Specimen 1 RGB, based on CSL statistics, was Σ47b with a misorientation angle of 57.125°. Specimen 2 RGB is Σ43c based on frequency percentage of CLS boundaries given in the histogram statistics.

FEI 3D Quanta was used to lift out the grain boundaries using a typical beam current ranging from 2.3 nA to 7 nA and beam energies of 30 kV and 5 kV for milling and cleanup, respectively. Each GB was approximately 20 μm in length and produced 10–12 atom probe tips. The SEM images of the tip preparation for specimen 1 are shown in Figures 1(b), 1(c), 1(f), and 1(g), and those for specimen 2 are shown in Figures 2(b), 2(c), 2(f), and 2(g).

APT studies were conducted on an IMAGO (Cameca) LEAP 3000X-Si. LEAP provides the required sensitivity and resolution (spatial resolution of 0.1 nm–0.5 nm) to study intergranular segregation at the atomic level [25]. An atom probe field evaporates individual atoms by applying standing voltage to a needle-shaped specimen (<50 nm radius) overlaid with short laser pulses that cause ionization [24]. The emitted ions hit a position sensitive detector and this coupled with time-of-flight mass spectrometry provides the positions and chemical identities for a 3D atom-by-atom LEAP

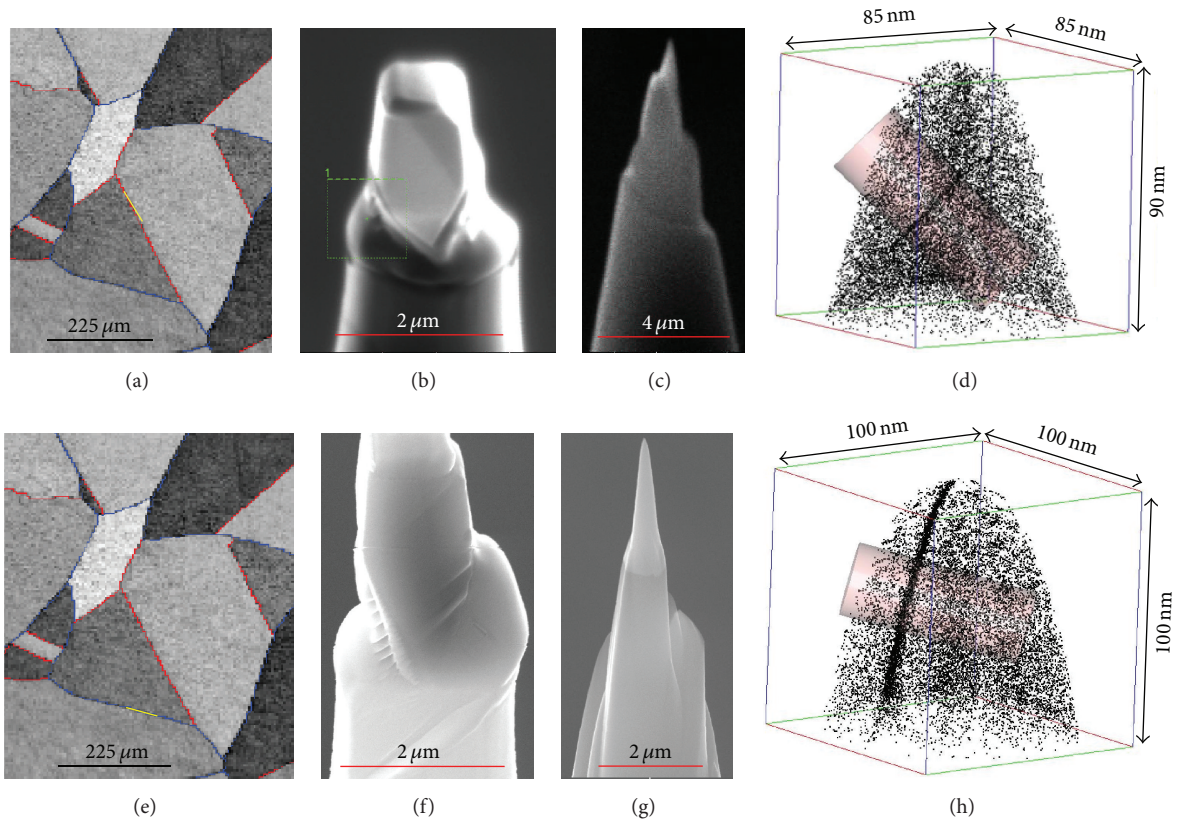

FIGURE 1: (a) Specimen 1 EBSD GB maps identifying the SGB (in red) extracted for analysis (location of extraction highlighted in yellow). (b-c) Specimen 1 SGB SEM images of the FIB preparation of the APT tip. (d) Specimen 1 SGB 3D atom-by-atom LEAP tomography reconstruction showing the cylindrical ROI for analysis (ions shown are Si only; 100% of ions are shown). (e) Specimen 1 EBSD GB maps identifying the RGB (in blue) extracted for analysis (location of extraction highlighted in yellow). (f-g) Specimen 1 RGB SEM images of the FIB preparation of the APT tip. (h) Specimen 1 RGB 3D atom-by-atom LEAP tomography reconstruction showing the cylindrical ROI for analysis (ions shown are Si only; 100% of ions are shown).

tomographic reconstruction of the specimen at the atomic level [24, 25] shown in Figures 1(d), 1(h), 2(d), and 2(h). Silicon and boron ions are simply chosen to best highlight the GB in the reconstructions. All 3D reconstructions presented in this study have a point size of 1.5. APT studies were conducted in laser mode at a pulse repetition rate of 200 kHz at a pulse energy of 0.20 nJ under ultrahigh vacuum maintaining a temperature of 40 K at the specimen tip utilizing a green (532 nm) laser pulse. Data analyses were performed using IVAS 3.6.6 software program. The GB locations provided in each data set of this study are given in ranges as the GB is not always positioned in a straight line. The cylindrical regions of interest (ROIs) for all specimens in this study were sized the same at ~28 nm diameter and ~70 nm length (z-direction) with the analysis in z-direction.

ROIs encompassing the GB and the matrix on either side were analyzed for this study as well. A rectangular prism ROI was divided into 1 nm slices and analyzed across the array parallel to the GB. Resultant 1D compositional profile graphs were developed from this data.

3. Results and Discussion

3.1. GBC Influence on Segregation to SGBs and RGBs. Figure 3(a) displays 3D atom-by-atom LEAP tomography reconstructions of each element identified using the IVAS 3.6.6 analysis software in specimen 1 SGB and Figure 3(b) displays specimen 1 RGB. It can be noted that, qualitatively, the SGB is more difficult to identify than the RGB if the segregation itself is used as a visual aid. As is seen in the SGB, figures are more reflective of the grain boundary mismatch versus actual segregation to the grain boundary except in the case of Si. Figure 3(b) displays 3D atom-by-atom LEAP tomography reconstructions of the random GB, where it shows nearly all elements segregated to the GB. It is also qualitatively evident that there is a greater concentration of segregants at the RGB. The special GB images in Figure 3(a) include 100% of the ions except for Ni which includes 0.1% of the ions and Al which includes only 50% of the ions as the image becomes too saturated. The random GB images in Figure 3(b) include 100% of the ions except for Ni at 0.1%, Si at 50%, and Al at 50%.

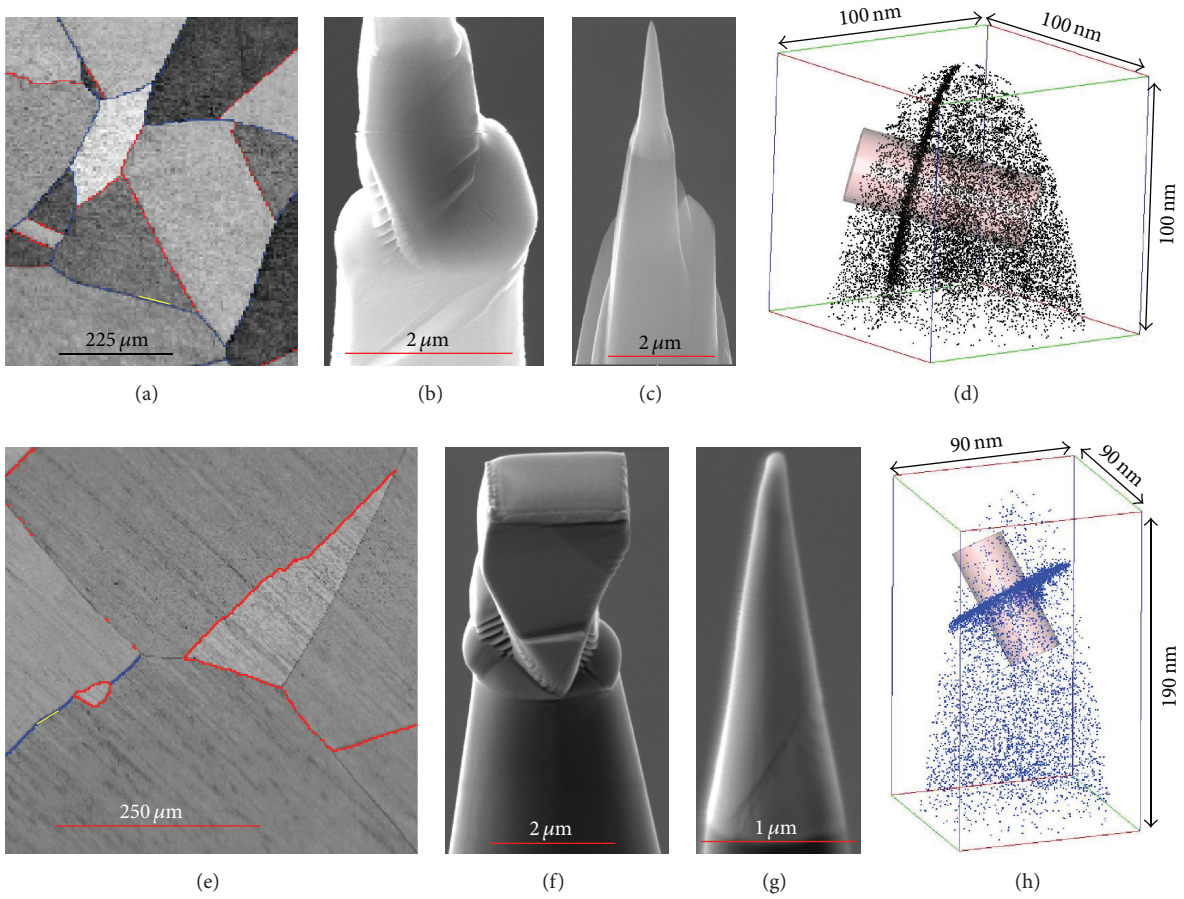

Figure 2: (a) Specimen 1 EBSD GB maps identifying the RGB (in blue) extracted for analysis (location of extraction highlighted in yellow). (b-c) Specimen 1 RGB SEM images of the FIB preparation of the APT tip. (d) Specimen 1 RGB 3D atom-by-atom LEAP tomography reconstruction showing the cylindrical ROI for analysis (ions shown are Si only; 100% of ions shown). (e) Specimen 2 EBSD GB maps identifying the RGB (in blue) extracted for analysis (location of extraction highlighted in yellow). (f-g) Specimen 2 RGB SEM images of the FIB preparation of the APT tip. (h) Specimen 2 RGB 3D atom-by-atom LEAP tomography reconstruction showing the cylindrical ROI for analysis (ions shown are B only; 100% of ions shown).

A quantitative comparison of the segregation of all impurities between the RGB and SGB was evaluated by identifying a region of interest (ROI) demarcated by the cylindrical volumes that pass perpendicularly through each GB within the 3D atom-by-atom LEAP tomography reconstructions shown in Figure 1(d) so that only the atoms in the ROIs were analyzed. This ROI encompassed the GB and bulk region of the sample such that the concentration of any atoms at the GB could be quantified with resultant 1D concentration profile graphs. Bulk compositions of the ROIs in both grain boundaries of specimen 1 are shown in Table 2. 1D concentration profile graphs of all the elements are displayed in Figures 4(a) and 4(b).

Figure 4(a) displays the 1D concentration profile for the SGB and it is evident that the only increase in concentration at the special GB, located at ~33 nm, is in silicon. Aluminum is shown as it has equal concentration to that of silicon. Elemental oxygen and carbon were also analyzed and no increase in concentration was found at the GB. However, there is a 46% increase in the amount of silicon segregated to the RGB shown in Figure 4(b) compared to the SGB in Figure 4(a). Figure 4(b) displays the 1D concentration profile for the RGB. The number of silicon atoms in each GB was nearly identical with 3,590 atoms in the SGB and 3,684 atoms in the RGB. The concentration of Si in the SGB was 0.43 at.% with a standard deviation of 0.039%, while the concentration of Si in the RGB was 0.80 at.% with a standard deviation of 0.059%. There is no enrichment of any other elements in the SGB. The RGB, however, provides clear evidence that all the segregants are enriched at the random GB located at approximately 45–46 nm.

This significant segregation of elements at the random GB and the lack of segregation, or reduced segregation in the case of Si, at the special GB provide evidence at the atomic level that special grain boundaries, specifically Σ3, do inhibit segregation of elements. The exception is silicon, although the concentration is half of that found in the RGB, which correlates with studies on segregation enthalpies of various

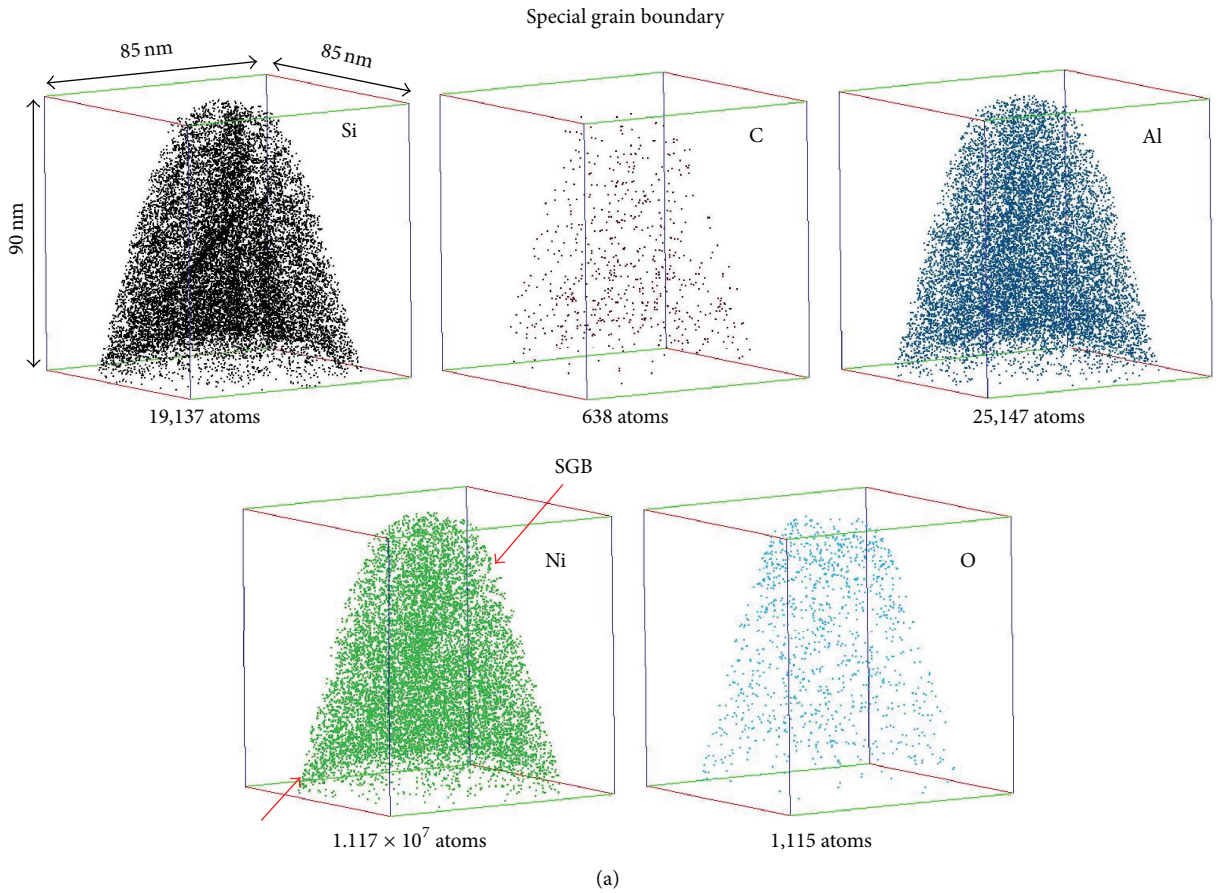

(a)

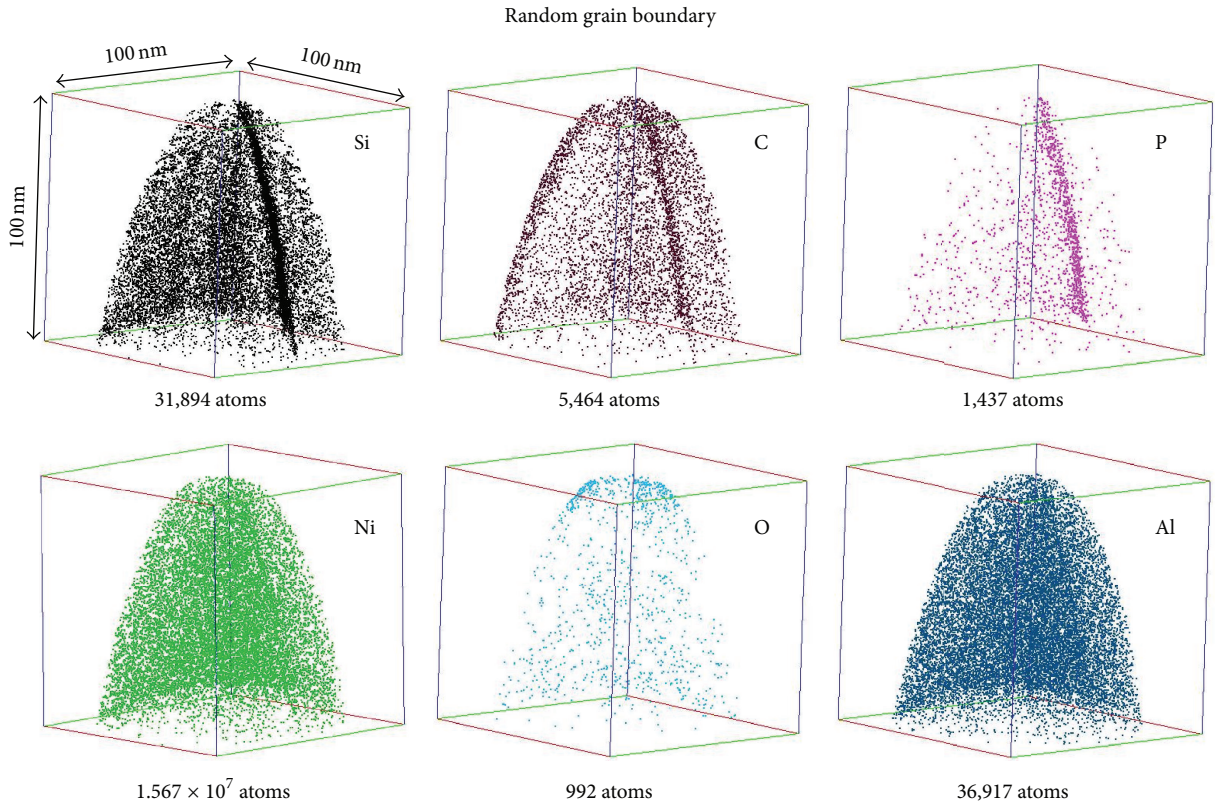

Figure 3: Continued.

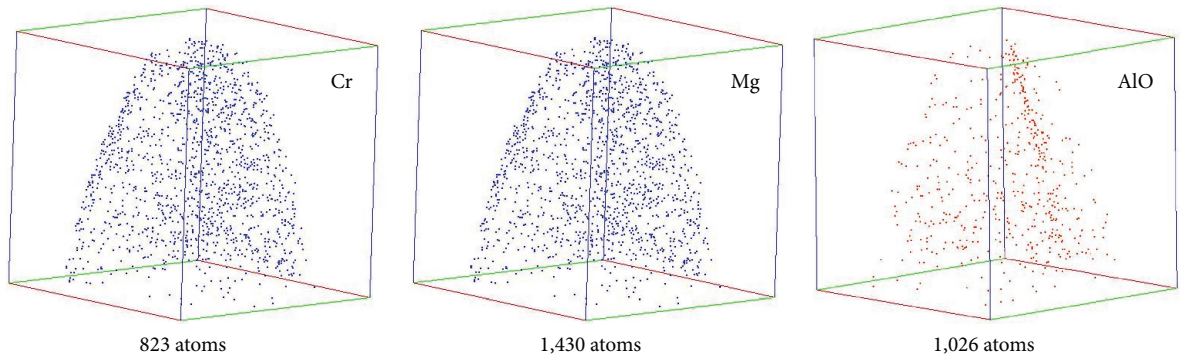

Figure 3: (a) 3D atom-by-atom LEAP reconstructions of specimen 1 SGB; point size = 1.5 and the percentage of ions shown is 100% except for Ni (0.1%) and Al (50%). (b) 3D reconstructions of specimen 1 RGB; point size = 1.5 and the percentage of ions shown is 100% except for Ni at 0.10%, Al at 50%, and Si at 50%.

Table 2: RGB and SGB ROI bulk compositions of specimen 1.

RGB			SGB		
Ion type	Count (atomic)	Ranged	Ion type	Count (atomic)	Ranged
Al	4513.0	0.2273%	Al	4649.0	0.2277%
Si	3684.0	0.1855%	Si	3590.0	0.1758%
Ni	1975573.0	99.4936%	Ni	2032126.0	99.5377%
O	65.0	0.0033%	O	126.0	0.0062%
C	449.0	0.0226%	C	120.0	0.0059%
P	232.0	0.0117%			
AlO	86.0	0.0043%			
Cr	51.0	0.0026%			
Mg	122.0	0.0061%			

elements [26]. Compared to carbon (−40 kJ/mol), silicon has segregation enthalpy of about −9 kJ/mol at a given grain boundary orientation so silicon has been shown to readily segregate at both random and special GBs but, as discussed, the SGB concentration in this experiment was about half of that in the RGB [27].

This lower tendency for segregation at the SGB is due to a lower grain boundary energy which translates to lower diffusivity for Σ3 boundary. GB energy for Σ3 is on the order of $<0.1\,J/m^2$ compared to a high angle random grain boundary of $>0.4\,J/m^2$ [8, 28]. This segregation resistance is because Σ3, a special boundary, has the largest number of coinciding lattice points, lower GB interfacial energy, and hindered GB migration [15].

First, the large number of coinciding lattice points translates into a more ordered structure and low free volume since one out of every three sites between the two grains coincides [8]. This ordered structure has high boundary cohesion with reduced dislocations and vacancies since SGBs act as barriers to dislocations [20]. This high number of coinciding atoms also corresponds to a minimum GB interfacial energy and leads to Σ3 boundary having about one-tenth the energy of any other CSL boundary [8]. The segregation resistance is driven by this lower interface energy as segregation occurs to reduce the overall energy of a system [29]; however, it is crucial to remember that a grain boundary itself is a defect and will provide a pathway for some amount of segregation. This segregation may be undetectable and may be in extremely low quantities but its relative behavior to RGB segregation is the subject of this study. Therefore, the minimum available energy of Σ3 boundary provides little driving force required for diffusion, when compared to a RGB, while the ordered structure results in a slower diffusion because vacancies need to move in a coordinated manner that preserves ordering [8]. This describes the relationship between GB diffusion coefficients and GB energies, where low energy grain boundaries have lower diffusion coefficients, which translates to the lower segregation amounts.

Second, segregation resistance in the SGB is caused by the inhibited GB migration due to the large fraction of Σ3 boundaries [14]. The abundance of Σ3s can be explained by their low stacking fault energy (SFE). Low SFE materials, such as Ni, readily form Σ3s during thermomechanical processing exhibiting high fractions of these boundaries because low SFE materials have an abundance of very wide stacking faults or interruptions in the stacking sequence of the crystal, and this inhibits dislocation movement (cross-slip and climb) and subsequently GB migration which is why Σ3s act as good

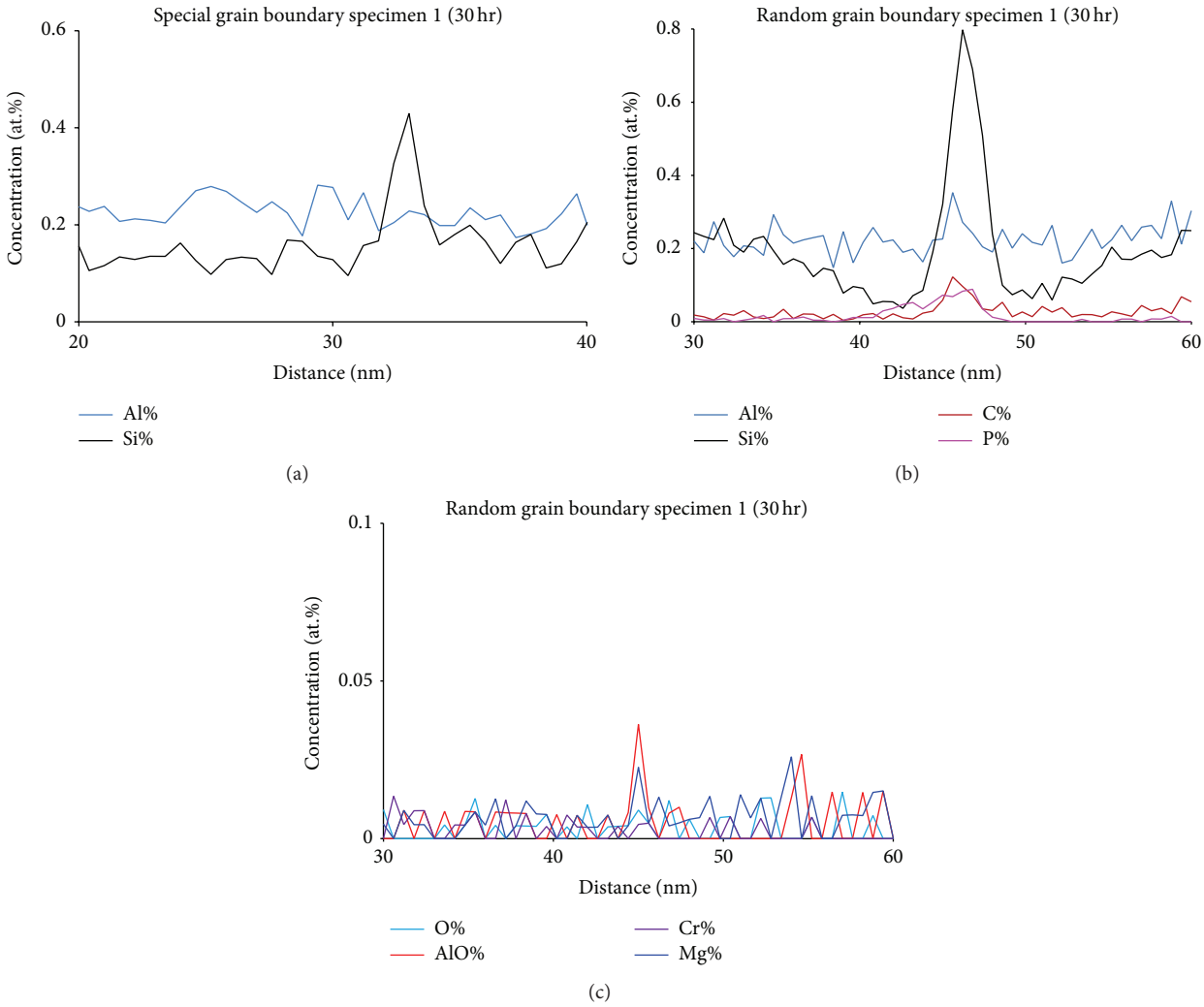

FIGURE 4: (a) 1D concentration profile graphs for the special GB of specimen 1. (b) 1D concentration profile graphs for Al, Si, C, and P for the random GB of specimen 1. (c) 1D concentration profile graphs for O, AlO, Cr, and Mg for the random GB of specimen 1.

barriers to dislocations [2, 30, 31]. The slower GB migration also nucleates Σ3s more readily. This abundance in stacking faults equates to an abundance of Σ3s.

To further investigate the silicon enrichment at the SGB, another ROI (rectangular prism) of 30 nm × 30 nm × 50 nm was extracted from this specimen. This procedure extracts fewer ions and therefore identifies elements that are present in very low concentration. These would not necessarily show up in the entire spectrum because of various background issues.

This ROI encompassed the GB and the matrix on either side as shown in Figure 5(a) and is highlighted in yellow (only Si atoms are shown for visualization of the GB). The GB is located at 11–16 nm, as shown in Figure 5(b), due to the curvature of the boundary within the analyzed region. The rectangular prism ROI is divided into 1 nm slices and was analyzed across the array parallel to the GB. The resultant 1D compositional profile graph still shows a concentration of Si at the GB approximately 54% higher than Si concentration in the bulk 10–15 nm out from the GB in both directions as shown in Figure 5(c). Again, the concentration at the RGB is still 46% higher than that in the SGB providing evidence that the special Σ3 GB does inhibit segregation at the GB. This could also indicate that the segregation enthalpy for Si in Ni is enough to overcome the low energy and ordered structure at the special GB to some extent. It has been found in some Ni alloys that Si does have a higher segregation tendency than even B or C as shown in Figures 5(c) and 5(d) for Si and C comparison [32]. The higher the energy state of a solute atom in the bulk, the higher the driving force for segregation, which could mean that Si has lower bulk solubility leading to propensity to segregate more readily in nickel even in the presence of SGB [9]. GB Engineering and the control of Si segregation could lead to additional improved performance in metal alloys as Si already reduces the effects of embrittlement [33]. Moreover, no typical embrittling elements, such as C and P, were enriched at the SGB suggesting that this is another mechanism by which SGBs can improve material performance.

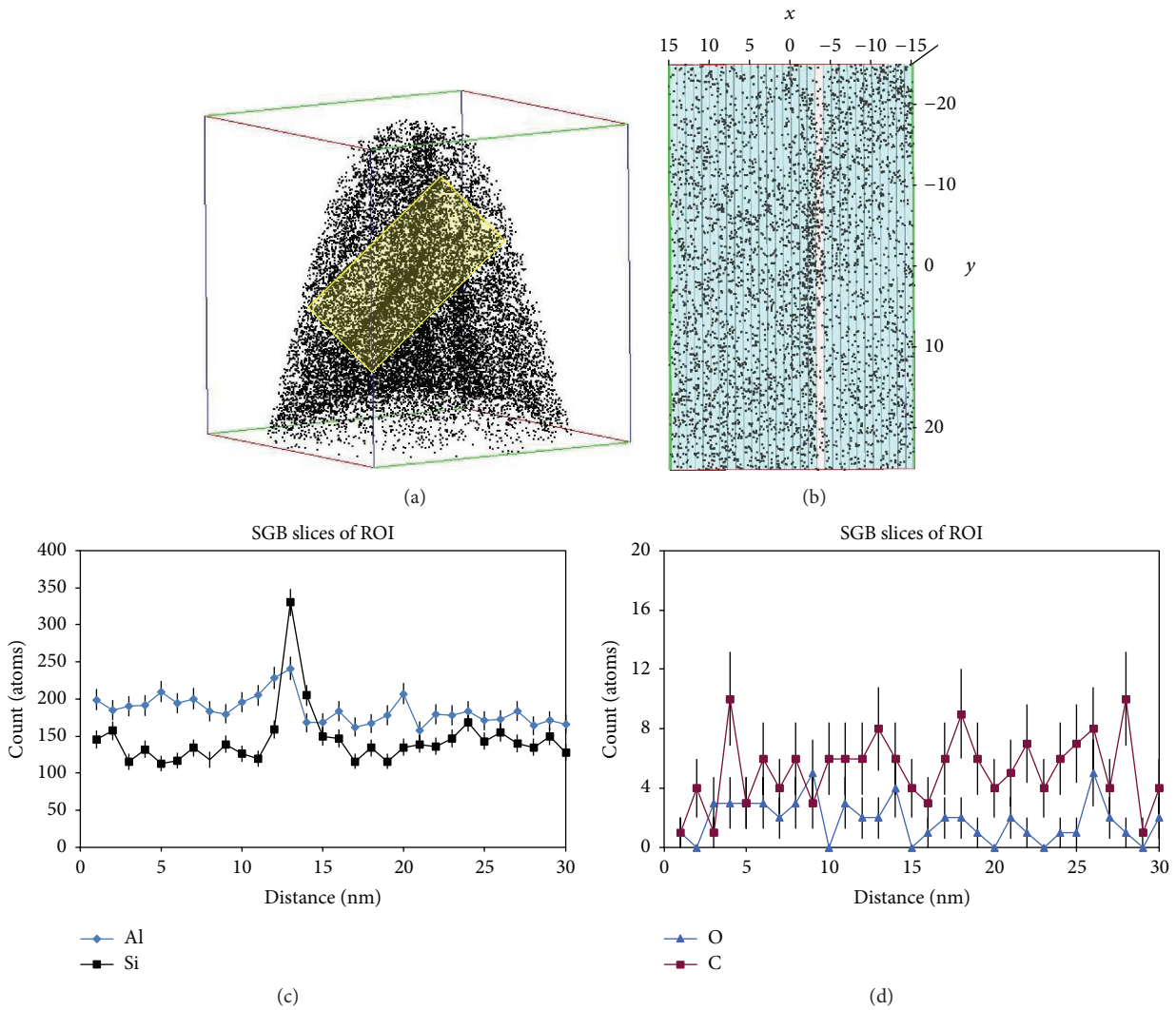

Figure 5: (a) The atom-by-atom 3D reconstruction with a representation of the rectangular prism ROI in yellow. (b) The IVAS image of the one-nanometer slices of the rectangular prism. (c) The concentration in atomic counts of the segregants (Al and Si) of the ROI for the SGB. (d) The concentration in atomic counts of the segregants (O and C) of the ROI for the SGB.

This same analysis on the RGB was done for further quantification and identification of other possible segregants. Figures 6(c)–6(e) show that all the impurities, except Cr and O, segregate to the RGB. In addition, Mn, Ni oxides, and Si oxides were identified and shown to be enriched as well. The lack of segregation of Cr could indicate that bulk solubilities or interfacial energies between segregants are in play. The carbon content can also affect the segregation behavior of elements (specifically their diffusion behavior in the bulk) and the RGB does contain about 73% more C than the SGB but, at these low concentrations, the errors are large [34].

3.2. Influence of Increased Annealing Time on Segregation of RGBs. The random grain boundaries from specimens 1 (annealed for 30 hours) and 2 (annealed for one hour) were studied by evaluating the effect of increased annealing times at 1000°C on segregation levels at random grain boundaries.

Figure 7 displays 3D atom-by-atom LEAP tomography reconstructions of each element identified in the RGB of specimen 2. Figure 3(b) displays the same for the RGB of specimen 1.

A quantitative comparison of the segregation of all impurities was evaluated by identifying a region of interest (ROI) demarcated by the cylindrical volumes that pass perpendicularly through each GB within the 3D atom-by-atom LEAP tomography reconstructions shown in Figures 2(d) and 2(h) so that only the atoms in the ROIs were analyzed. The ROI encompassed the GB and bulk region of the sample such that the concentration of any atoms at the GB could be quantified with resultant 1D concentration profile graphs. The cylindrical ROIs for all specimens in this study were sized the same at ~28 nm diameter and ~70 nm length (z-direction) with the analysis in z-direction. Bulk compositions of the cylindrical ROIs from specimens 1 and 2 are shown in Table 3. Subsequently, 1D concentration profile

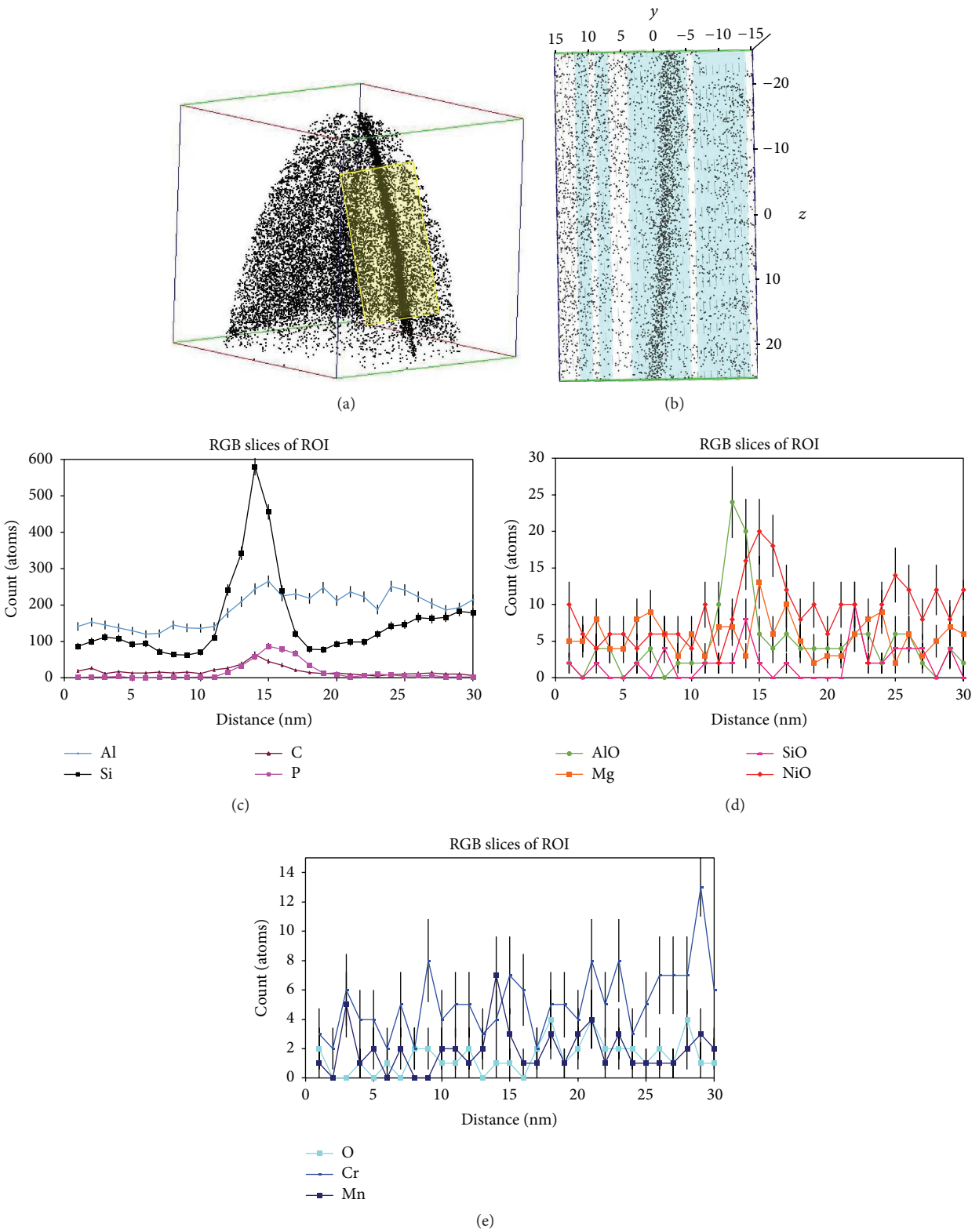

Figure 6: (a) The atom-by-atom 3D reconstruction with a representation of the rectangular prism ROI in yellow. (b) The IVAS image of the one-nanometer slices of the rectangular prism. (c) The concentration in atomic counts of the segregants (Al, Si, C, and P) of the ROI for the RGB. (d) The concentration in atomic counts of the segregants (AlO, Mg, SiO, and NiO) of the ROI for the RGB. (e) The concentration in atomic counts of the segregants (O, Cr, and Mn) of the ROI for the RGB.

Table 3: RGB ROI bulk compositions (atomic) for specimens 1 and 2, respectively.

	Specimen 1 RGB			Specimen 2 RGB	
Ion type	Count (atomic)	Ranged	Ion type	Count (atomic)	Ranged
Al	4513	0.2273%	Al	5263.0	0.2238%
Si	3684	0.1855%	Si	3824.0	0.1626%
Ni	1975573	99.4936%	Ni	2340822.0	99.5411%
O	65	0.0033%	O	30.0	0.0013%
C	449	0.0226%	C	403.0	0.0171%
P	232	0.0117%	P	49.0	0.0021%
AlO	86	0.0043%	B	1030.0	0.0438%
Cr	51	0.0026%	Cr	89.0	0.0038%
Mg	122	0.0061%	Mg	103.0	0.0044%

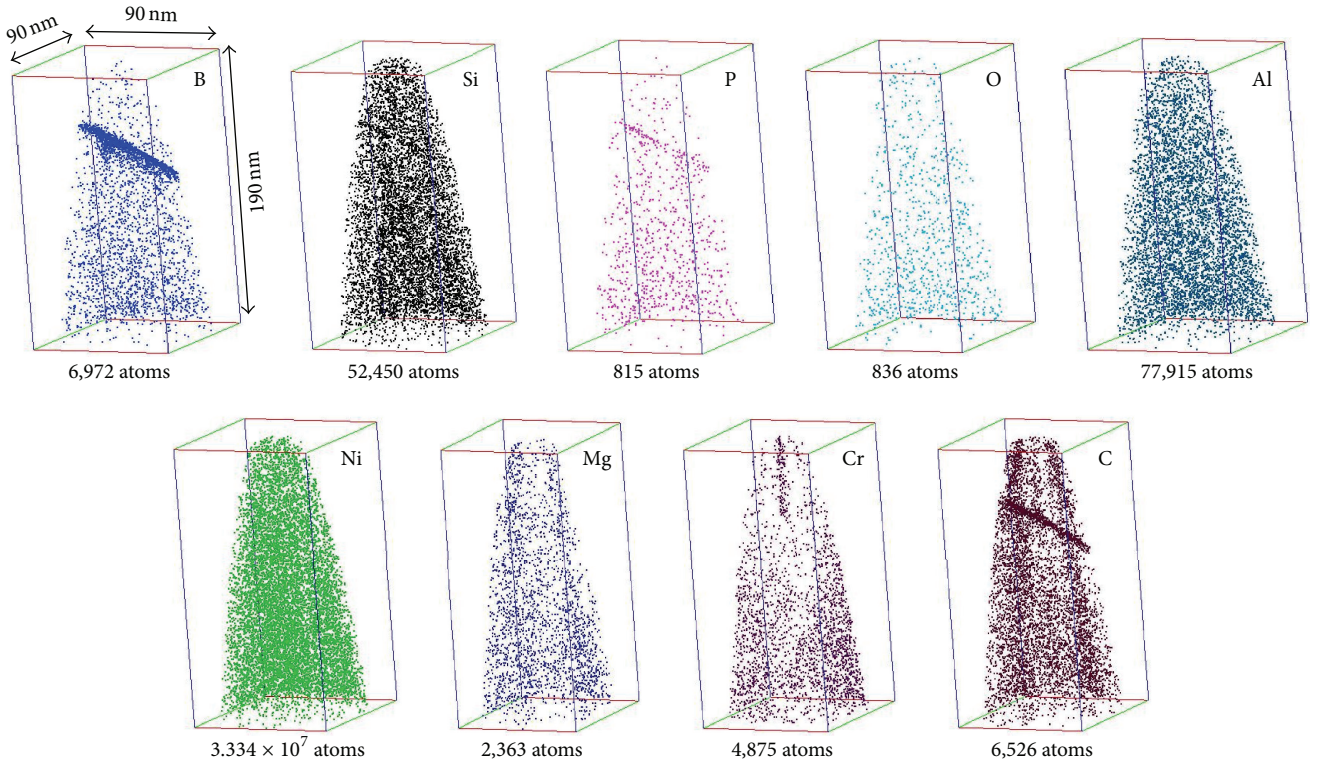

Figure 7: Atom probe tomography reconstructions of the RGB in specimen 2 (annealed for one hour); point size = 1.5 and the percentage of ions shown is 100% except for Ni (0.03%), Si (15%), Cr (50%), B (50%), and Al (7%).

graphs of all the elements were developed and are displayed in Figure 8.

As shown in Figure 4(b) and discussed in Section 3.1, the RGB from specimen 1, annealed for 30 hours, exhibits enrichment of all segregants at the GB except Cr. Specimen 2 RGB was only annealed for one hour and the 1D concentration profile graphs are shown in Figure 8 with various y-scales to better show the concentration enrichment or lack thereof at the random GB. The dotted line provides the GB location at 31.2 nm–32.4 nm through the cylindrical ROI with analysis in z-direction.

Figures 8(a), 8(d), and 8(e) provide the 1D concentration profiles of Al, Si, Mg, and Cr, where it can be seen that these elements are not enriched at the random GB, whereas P, B, and C in Figures 8(b) and 8(c) are shown to be enriched at the random GB. This observed behavior for Al, Si, Mg, and Cr indicates that complex grain boundary migration processes and/or site competition have roles in GB enrichment at the RGB.

Although this phenomenon is more likely due to complex grain boundary migration processes, this enrichment could also be due to physical site competition, which warrants some

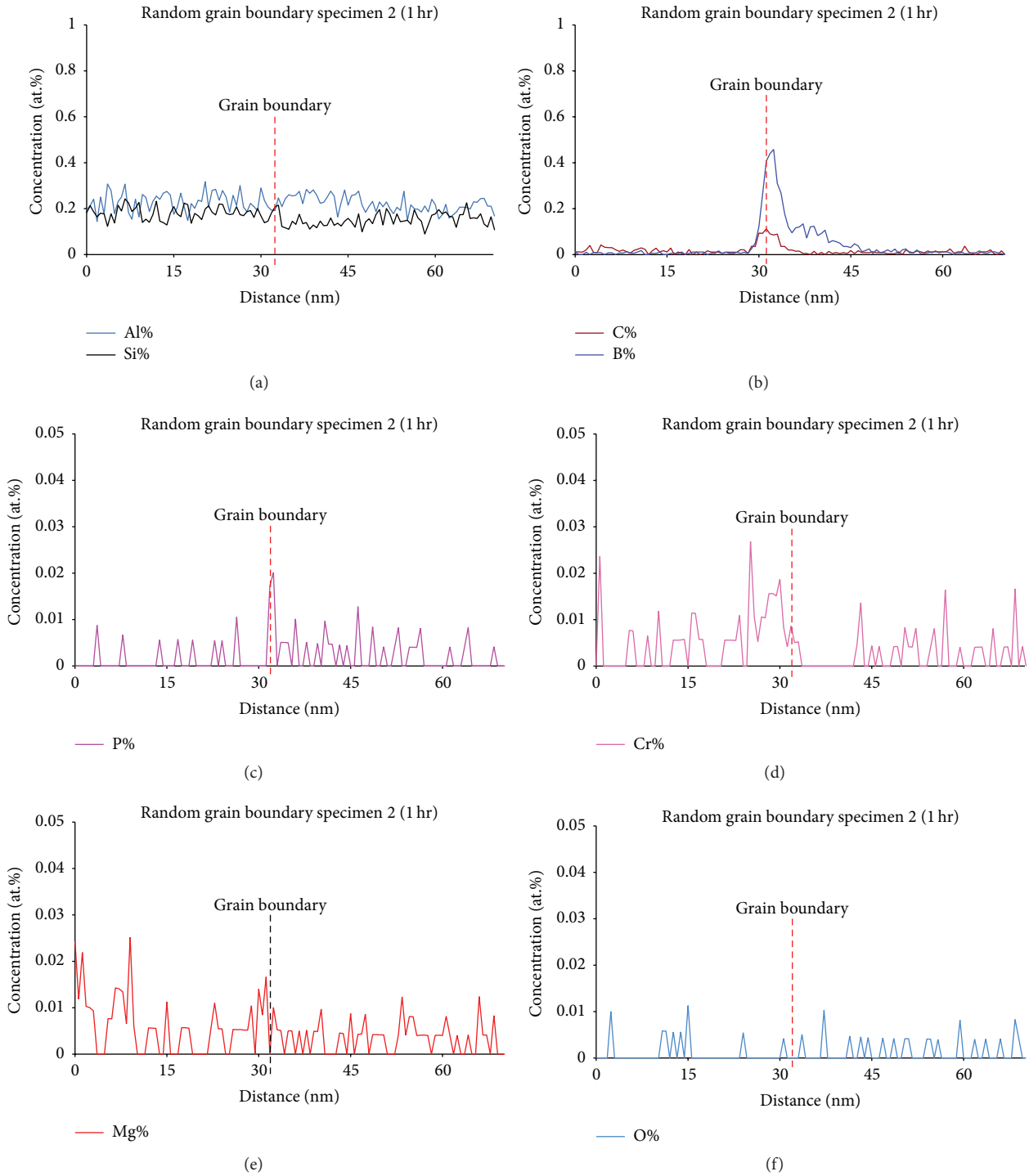

Figure 8: RGB of specimen 2 1D concentration profile graphs: (a) Al and Si, (b) C and B, (c) P, (d) Cr, (e) Mg, and (f) O.

discussion. The atomic radii of P, B, and C are small as seen in Table 4 (98 pm, 87 pm, and 67 pm, resp.), where they can take advantage of relatively smaller vacancies or interstitial sites available for diffusion as these are interstitial elements [7]. Si, Mg, Cr, and Al are much larger (111 pm, 145 pm, 166 pm, and 118 pm, resp.) which may be too large (atomic radius of Ni is 149 pm) to take advantage of these available sites in addition to the inability to compete with the diffusion of the smaller atoms. Interstitial diffusion is faster than vacancy diffusion and the smaller impurity atoms mentioned above could therefore diffuse into the interstitial sites in the GB leaving no space for diffusion of the larger atomic radii impurity atoms. It has been found in some Ni alloys that Si does have a higher segregation tendency than even B or C

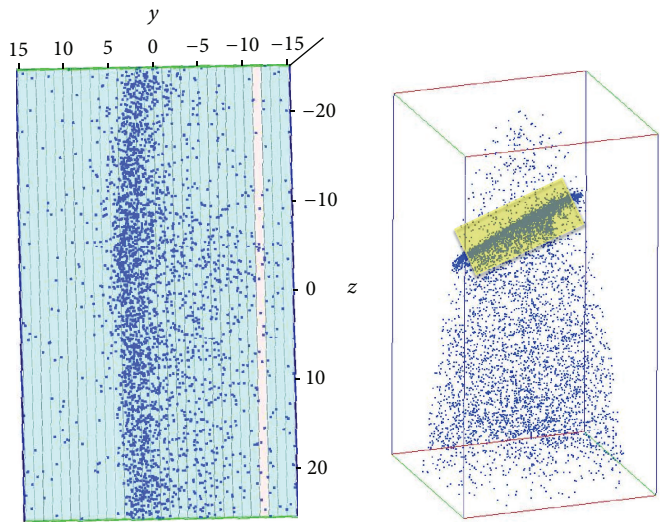

Figure 9: Atom-by-atom 3D reconstruction with a representation of the rectangular prism ROI in yellow (b) and the IVAS image of the one-nanometer slices of the rectangular prism (a) analyzed (atoms shown in image are B only).

Table 4: Atomic radii of all Ni elements and impurities.

Element	Atomic radius (pm)
Ni	149
C	67
Cu	145
Fe	156
Mn	161
S	88
Si	111
Al	118
B	87
Cr	166
Co	152
Mg	145
P	98
V	171

[32] but, interestingly, the behavior of these elements in this study suggests that this tendency may be overcome by other grain boundary interactions or processes such as physical site competition.

However, as mentioned above, the differences in segregation of these elements within the same specimen are more likely due to complex high temperature grain boundary migration processes and interactions. Annealing increases grain boundary migration, which in turn affects segregation behavior and diffusion processes [35]. There are a host of driving forces that affect grain boundary migration which in turn can affect segregation behavior such as temperature, grain boundary thickness, and drag effects caused by the segregants having to be carried along during migration and, in turn, the segregants' inability to maintain their position within the grain boundary as it migrates [36]. As far as temperature effects are concerned, the shorter annealing time of one hour may not have been enough time to drive the segregation of these elements. Another possibility is that these elements (Si, Mg, Cr, and Al) did initially segregate to the grain boundary but due to drag effects were unable to maintain their positions within the grain boundary during migration [36]. Other possible interactions include a potential preferential interaction of these nonsegregating elements due to the presence of B in specimen 2 which does not exist in specimen 1 [34].

Figure 8(f) shows that O is not enriched at the GB. Elemental oxygen, in this case, is not expected to be segregated to the GB but distributed evenly throughout the sample. However, oxides would be expected to be enriched at the random GB but none were identified in this analysis of this specimen. This is most likely due to the shorter annealing time as well as the difficulty in identifying oxides, particularly nickel oxides, as the noise ceiling and width of the Ni peaks in the mass spectrum could camouflage these oxides.

To further investigate the lack of segregation of Si, Mg, Cr, and Al in the RGB of specimen 2, another ROI (rectangular prism) of 30 nm × 30 nm × 50 nm was exported from this specimen in IVAS which encompassed the GB and bulk matrix on either side as shown in Figure 9. Thin one-nanometer slices, parallel to the GB, were analyzed individually. The atoms shown in the IVAS image are B for better visualization of the rectangular prism ROI.

First, segregants not previously identified in the initial analyses shown in the paper thus far were found in this ROI such as B, NiO_2, and Fe. Second, Figure 10(a) shows that Si and Al are indeed segregated to the GB as would be expected in a random GB. Figures 10(a) and 10(b) display the number of atoms per one-nanometer slice in the ROI and also show that C, B, P, AlO, and NiO_2 are segregated to the GB

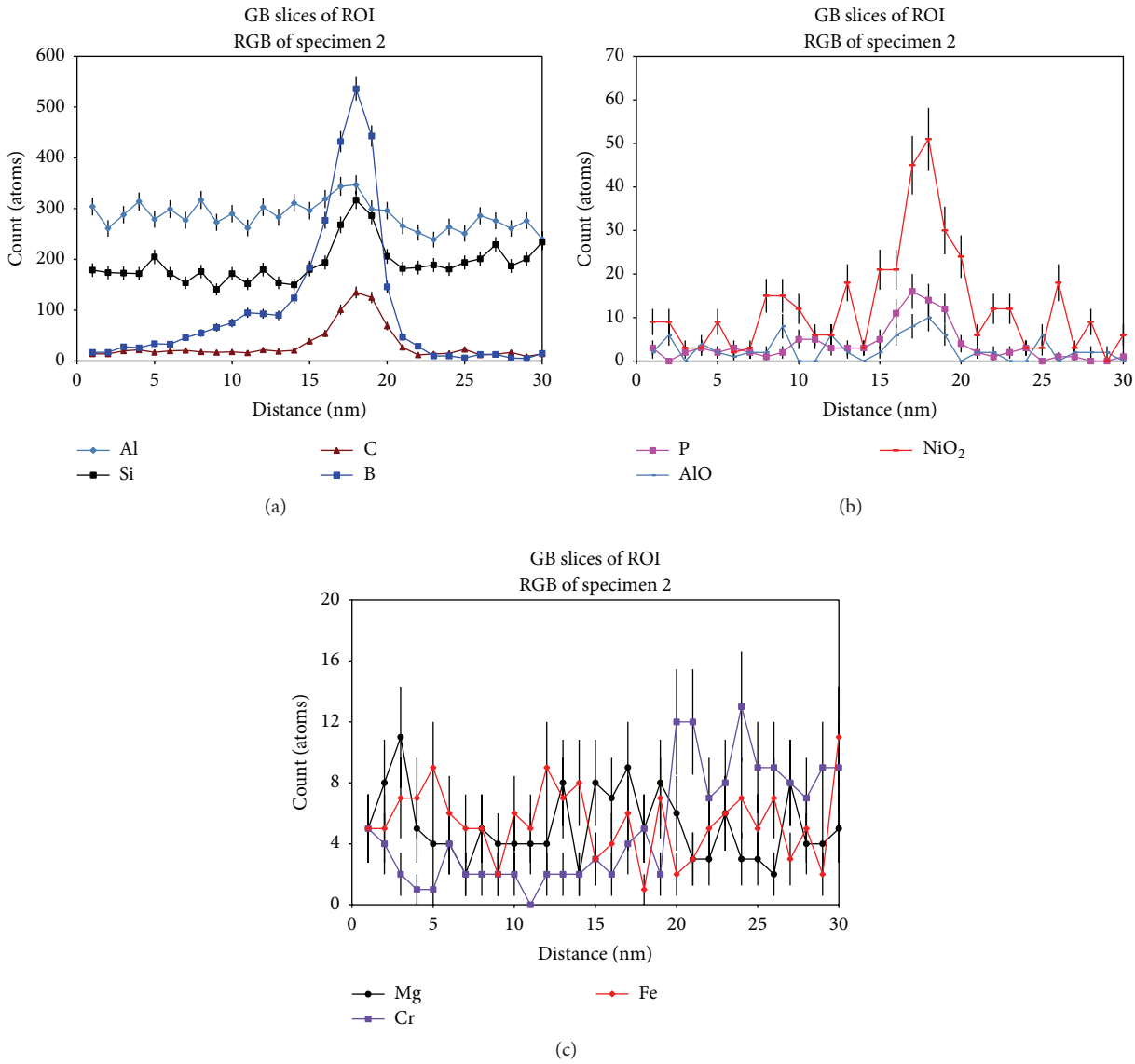

FIGURE 10: The concentration in atomic counts against the distance across the ROI (rectangular prism) of the segregants in the RGB of specimen 2 for (a) Al, Si, C, and B; (b) P, AlO, and NiO_2; (c) Mg, Cr, and Fe.

as would be expected. The GB is located at approximately 17–19 nm. Third, Figure 10(c) shows that the concentrations of Mg, Cr, and Fe do slightly increase directly at the GB but these increased concentrations are not higher than other locations within the bulk. Again, there are a multitude of high temperature grain boundary migration interactions that are likely responsible for this segregation behavior. The atomic radii of Mg, Cr, and Fe (145 pm, 166 pm, and 156 pm, resp.) are much larger than Si and Al (111 pm and 118 pm, resp.) which could allow for segregation or diffusion of Si and Al to the random GB more easily. However, the larger atomic radii elements may have initially segregated to the grain boundary but due to other interactions, such as size of atoms/grain boundary or bonding, may not have been able to hold their positions within the grain boundary during migration [36].

In this study, increased annealing time does show an increase in the amount of segregation of some elements at the random GB as would be expected since an increase in annealing time at 1000°C would provide significant driving force for segregation. Si and Al, the main impurity elements in Ni, exhibit a 74% and 43% increase, respectively, in their concentration at the RGB from one-hour annealing to 30-hour annealing. The standard deviation is shown in Table 5. The remaining errors become larger as the atomic percent concentrations become smaller. Phosphorous content also increases by 77% at the RGB with increased annealing time. These results provide evidence that an increase in annealing

Table 5: Standard deviations (in units of percentage since the data is in units of percentage).

Specimen	At.% Si	At.% Al
Specimen 1	0.059	0.042
Specimen 2	0.034	0.029

time does drive a higher percentage of most segregants to a random GB.

4. Conclusions

This study successfully used EBSD GB maps to identify and lift out type-specific grain boundaries to study segregation behavior of Ni at the atomic level using APT. The significant findings and observations are listed as follows:

(i) Σ3 SGBs do inhibit segregation of impurities at the GB compared to RGBs in Ni under the current research conditions.

(ii) The evidence in this research suggests that increasing annealing time from 1 hour to 30 hours for RGBs does increase the concentration of segregants at the GB.

The 1000°C annealing for 30 hours should have been a driving force for segregation but the SGB still showed very little quantified data providing evidence of segregation. Some Ni-based superalloys in some gas turbine components can experience temperatures in the range of 650°C to over 1000°C [37]. The lack of segregation in the SGB even after 1000°C strongly indicates that Σ3 type of SGB is very effective in retarding segregation of impurities at the GB. Consequently, a higher fraction of special grain boundaries is desirable in enhancing material performance due to increased segregation resistance.

The role of segregants at grain boundaries is not well understood and certainly not well quantified. There are questions concerning segregants and their interactions with one another and their interactions with type-specific grain boundaries [4]. This quantitative assessment used APT which has both the chemical sensitivity and resolution capability of studying segregation behavior at grain boundaries. This atomic level study has provided quantitative data and observations about GB segregation in Ni regarding the GB character influence on segregation behavior.

This insight will feed future efforts in better understanding segregation behavior as well as the structure of type-specific grain boundaries during segregation in materials for performance improvement in countless applications.

Future work in this area of study could incorporate texture analysis to include the identification of the dominant crystal orientations of each type-specific grain boundary to more completely describe and understand the boundary conditions. A better understanding of the diffusion process with respect to this texture analysis could provide additional insights into the segregation behavior at the atomic level. As grain boundary migration is a complex topic, more work is needed in understanding the mechanisms at play when discussing the driving forces that would cause some impurities/elements to segregate more than others within the same sample.

Disclaimer

Any opinions, findings, and conclusions or recommendations expressed in this material are those of the authors and do not necessarily reflect the views of the National Science Foundation.

Conflict of Interests

The authors declare that there is no conflict of interests regarding the publication of this paper.

Acknowledgments

This research is supported by the National Science Foundation under Grant no. DMR-1151109. The authors would like to thank Johnny Goodwin at the Central Analytical Facility, University of Alabama, Tuscaloosa, Alabama, for his expertise in the Electron Backscattered Diffraction and would also like to thank Chad Hornbuckle, University of Alabama, for his expertise in the local electrode atom probe. Professor Gregory B. Thompson and Dr. Monica Kapoor thank ARO-W911NF-13-1-0436 for support of this research.

References

[1] Y. Gao, R. O. Ritchie, M. Kumar, and R. K. Nalla, "High-cycle fatigue of nickel-based superalloy ME3 at ambient and elevated temperatures: Role of grain-boundary engineering," *Metallurgical and Materials Transactions A*, vol. 36, no. 12, pp. 3325–3333, 2005.

[2] B. M. Guyot and N. L. Richards, "A study on the effect of cold rolling and annealing on special grain boundary fractions in commercial-purity nickel," *Materials Science and Engineering: A*, vol. 395, no. 1-2, pp. 87–97, 2005.

[3] T. Watanabe, "An approach to grain boundary design for strong and ductile polycrystals," *Res Mechanica*, vol. 1, pp. 47–84, 1984.

[4] M. L. Taheri, J. T. Sebastian, B. W. Reed, D. N. Seidman, and A. D. Rollett, "Site-specific atomic scale analysis of solute segregation to a coincidence site lattice grain boundary," *Ultramicroscopy*, vol. 110, no. 4, pp. 278–284, 2010.

[5] V. Rothova, "Control of intergranular oxidation by thermal treatment," *Metal*, vol. 19–21, pp. 1–8, 2009.

[6] P. Lejcek and O. Schneeweiss, "Solute segregation at ordered grain boundaries," *Surface Science*, vol. 487, no. 1–3, pp. 210–222, 2001.

[7] D. N. Seidman, B. W. Krakauer, and D. Udler, "Atomic scale studies of solute-atom segregation at grain boundaries: experiments and simulations," *Journal of Physics and Chemistry of Solids*, vol. 55, no. 10, pp. 1035–1057, 1994.

[8] M. Meyers and K. Chawla, *Mechanical Behavior of Materials*, Cambridge University Press, New York, NY, USA, 2nd edition, 2009.

[9] P. Felfer, *Understanding Grain Boundary Segregation through Atom Probe Tomography*, The University of Sydney, New South Wales, Australia, 2012.

[10] C. J. Boehlert, S. C. Longanbach, and T. R. Bieler, "Effect of thermomechanical processing on the creep behaviour of Udimet alloy 188," *Philosophical Magazine*, vol. 88, no. 5, pp. 641–664, 2008.

[11] V. Randle, M. Coleman, and M. Waterton, "The role of Σ9 boundaries in grain boundary engineering," *Metallurgical and Materials Transactions A*, vol. 42, no. 3, pp. 582–586, 2010.

[12] V. Randle, "Twinning-related grain boundary engineering," *Acta Materialia*, vol. 52, no. 14, pp. 4067–4081, 2004.

[13] S. L. Yang, U. Krupp, H.-J. Christ, and V. B. Trindade, "The relationship between grain boundary character and the intergranular oxide distribution in IN718 superalloy," *Advanced Engineering Materials*, vol. 7, no. 8, pp. 723–726, 2005.

[14] S. L. Lee and N. L. Richards, "The effect of single-step low strain and annealing of nickel on grain boundary character," *Materials Science and Engineering A*, vol. 390, no. 1-2, pp. 81–87, 2005.

[15] V. Randle, *The Role of the Coincidence Site Lattice in Grain Boundary Engineering*, The Institute of Materials, Minerals and Mining, London, UK, 1996.

[16] B. Guyot, S.-L. Lee, and N. L. Richards, "Effect of small strain levels on special boundary distribution in commercially pure nickel," *Journal of Materials Engineering and Performance*, vol. 14, no. 1, pp. 85–90, 2005.

[17] Q. Li, J. R. Cahoon, and N. L. Richards, "Effects of thermomechanical processing parameters on the special boundary configurations of commercially pure nickel," *Materials Science and Engineering A*, vol. 527, no. 1-2, pp. 263–271, 2009.

[18] S. L. Lee and N. L. Richards, "Influence of long term annealing on grain boundary character distributions in nickel," *Materials Science and Engineering A*, vol. 405, no. 1-2, pp. 74–85, 2005.

[19] B. M. Guyot and N. L. Richards, "A preliminary model to predict the special grain boundary fraction in commercial-purity nickel," *Journal of Materials Processing Technology*, vol. 189, no. 1–3, pp. 162–168, 2007.

[20] E. M. Lehockey and G. Palumbo, "On the creep behaviour of grain boundary engineered nickel," *Materials Science and Engineering A*, vol. 237, no. 2, pp. 168–172, 1997.

[21] D. S. Lee, H. S. Ryoo, and S. K. Hwang, "A grain boundary engineering approach to promote special boundaries in Pb-base alloy," *Materials Science and Engineering A*, vol. 354, no. 1-2, pp. 106–111, 2003.

[22] P. J. Felfer, T. Alam, S. P. Ringer, and J. M. Cairney, "A reproducible method for damage-free site-specific preparation of atom probe tips from interfaces," *Microscopy Research and Technique*, vol. 75, no. 4, pp. 484–491, 2012.

[23] M. K. Miller and K. F. Russell, "Atom probe specimen preparation with a dual beam SEM/FIB miller," *Ultramicroscopy*, vol. 107, no. 9, pp. 761–766, 2007.

[24] M. K. Miller, *Atom Probe Tomography Analysis at the Atomic Level*, Kluwer Academic/Plenum Publishers, New York, NY, USA, 1st edition, 2000.

[25] K. Stiller, L. Viskari, G. Sundell et al., "Atom probe tomography of oxide scales," *Oxidation of Metals*, vol. 79, no. 3-4, pp. 227–238, 2013.

[26] P. Lejcek and S. Hofmann, "Segregation enthalpies of phosphorus, carbon and silicon at {013} and {012} symmetrical tilt grain boundaries in an Fe-3.5 at.% Si alloy," *Acta Metallurgica et Materialia*, vol. 39, no. 10, pp. 2469–2476, 1991.

[27] P. Lejcek, *Grain Boundary Segregation in Metals*, Springer, Heidelberg, Germany, 2010.

[28] P. Lejcek, "Grain boundary segregation in ordered alloys," in *Met*, Institute of Physics, Prague, Czech Republic, 2014.

[29] D. A. Porter and K. E. Easterling, *Phase Transformations in Metals and Alloys*, Chapman & Hall, New York, NY, USA, 2nd edition, 1992.

[30] D. L. Olmsted, S. M. Foiles, and E. A. Holm, "Survey of computed grain boundary properties in face-centered cubic metals: I. Grain boundary energy," *Acta Materialia*, vol. 57, no. 13, pp. 3694–3703, 2009.

[31] V. Randle, "Mechanism of twinning-induced grain boundary engineering in low stacking-fault energy materials," *Acta Materialia*, vol. 47, no. 15, pp. 4187–4196, 1999.

[32] D.-S. Wei, L. Shi, and Y.-R. Wang, "Experimental study on the cyclic mechanical behaviors of two Ni-based superalloys at elevated temperature," *Materials Science and Engineering: A*, vol. 569, pp. 124–131, 2013.

[33] C. Soontrapa, *Modeling stress accelerated grain boundary oxidation (SAGBO) in INCOLOY alloy 908 [M.S. thesis]*, Massachusetts Institute of Technology, 2005.

[34] T. Alam, P. J. Felfer, M. Chaturvedi, L. T. Stephenson, M. R. Kilburn, and J. M. Cairney, "Segregation of B, P, and C in the ni-based superalloy, Inconel 718," *Metallurgical and Materials Transactions A: Physical Metallurgy and Materials Science*, vol. 43, no. 7, pp. 2183–2191, 2012.

[35] Y. R. Kolobov, G. P. Grabovetskaya, M. B. Ivanov, A. P. Zhilyaev, and R. Z. Valiev, "Grain boundary diffusion characteristics of nanostructured nickel," *Scripta Materialia*, vol. 44, no. 6, pp. 873–878, 2001.

[36] G. Gottstein and L. S. Shvindlerman, *Grain Boundary Migration in Metals: Thermodynamics, Kinetics, Applications*, CRC Press, New York, NY, USA, 2nd edition, 2010.

[37] M. C. Kushan, S. C. Uzgur, Y. Uzunonat, and F. Diltemiz, "ALLVAC 718 Plus™ superalloy for aircraft engine applications," in *Recent Advances in Aircraft Technology*, R. K. Agarwal, Ed., chapter 4, pp. 75–96, InTech, Rijeka, Croatia, 2012.